




Microstructure and Mechanical Properties of AlCoCrFeNi High-Entropy Alloy-Reinforced Ti-Al Metallic-Intermetallic Composites

ENHAO WANG ,^{1,4} LISONG LV,¹ FUWEI KANG,^{1,5} YICEN ZHAO,¹ NANLIN LI,² YAO TIAN,³ and WEI JIANG¹

1.—School of Materials Science and Chemical Engineering, Harbin University of Science and Technology, Harbin 150040, China. 2.—Harbin Dong'an High Precision Tube Shaft Manufacturing Co. LTD, Harbin 150060, China. 3.—Xi'an Institute of Applied Optics, Xi'an 710065, China. 4.—e-mail: enhaowang@hrbeu.edu.cn. 5.—e-mail: fuwei_kang@163.com

In this study, a novel high-entropy alloy-reinforced Ti-Al metallic-intermetallic laminated (HEA-MIL) composite was fabricated using vacuum hot pressing sintering. The microstructure characteristics of the HEA-MIL composite interface were examined through X-ray diffraction, scanning electron microscopy, energy dispersive spectroscopy, and electron backscattered diffraction. The analysis revealed the presence of Al₃Ti, a newly formed phase in the HEA-MIL composite, resulting from the Ti-Al reaction and forming a homogeneous intermetallic compound layer. Furthermore, the HEA layer exhibited a body-centered cubic structure with a uniform stress distribution. Additionally, the mechanical properties of HEA-MIL composites were evaluated through compression tests conducted at quasi-static strain rates. The results revealed that the average compressive strengths of the HEA-MIL composite were 1359.61 MPa (load perpendicular to layers) and 1258.47 MPa (load parallel to layers), with corresponding failure strains of 41.53% and 17.84%, respectively. Fracture analysis demonstrated a mixed fracture mechanism, with both ductile and brittle fractures observed in both perpendicular and parallel directions.

INTRODUCTION

Intermetallic compounds have the excellent properties of high hardness, high strength, good corrosion resistance and low density. However, most intermetallic compounds lack a slip system at low temperature, so it is difficult for dislocations to move during deformation, resulting in low plasticity of the material, which greatly limits its application.^{1–3} In recent years, to solve the problem of poor plasticity of intermetallic compounds, a special structure of intermetallic compound laminated composites has been developed.^{4–6} Ti/Al₃Ti laminated (MIL) composite is one of the most promising materials in the field of aerospace and armor

protection, and it has been thoroughly investigated. For example, Rawer et al.^{7,8} used hot pressing sintering to prepare the first metal-intermetallic laminated composite. Their research showed that the material could change the phase composition and failure mechanism by changing the thickness ratio of the metal to the intermetallic compound. Vecchio et al.^{4,9–11} investigated the mechanical properties and crack propagation patterns of metal-metal layered composites, showing that MIL composites have the potential to become multifunctional materials by integrating the characteristics of metal-intermetallic compounds between layers. In addition to Ti/Al laminated composites, there are some new laminated composite systems based on the interlayer between ductile and brittle layers, such as Ni-Al^{12,13} and Ti-Mg^{14,15} systems.

To improve the mechanical properties of Ti-Al₃Ti MIL composites, it is a typical way to introduce reinforcements into MIL composites.^{16–19} For instance, Wang et al.^{20–22} introduced shape memory alloy (SMA) NiTi fiber/sheet as reinforcement in Ti/Al₃Ti MIL composite to improve its mechanical and functional properties. The results indicated that the introduction of NiTi fiber can significantly improve its damping performance, and the introduction of NiTi plate can improve its tensile and compressive properties. The NiTi/(Al₃Ti-Al₃Ni) MIL composite was prepared by replacing the Ti plate with NiTi plate. The tensile properties of the NiTi/(Al₃Ti + Al₃Ni) MIL composite showed high failure strain, and the average compressive strength when the load was perpendicular to the layer. In Han's work,^{23–25} ceramic Al₂O₃ and SMA NiTi hybrid fiber-reinforced Ti-Al metal-intermetallic laminated composite (CSMAFR-MIL), Ti-(Al₃Ti + Al₃Ni)/SiC_f-MIL composite and NiTi_f-SiC_f synergistically reinforced (Al₃Ti + Al₃Ni)-based metallic-intermetallic laminated (NiTi_f-SiC_f/(Al₃Ti + Al₃Ni)-MIL) composite were prepared using HP process in vacuum. The three materials have outstanding mechanical properties and good anti-crack propagation ability. These examples show that the transformation from single principal element reinforcement to multi-principal reinforcement of MIL composites is the key research object at this stage.

In traditional alloy systems, the main properties of alloys depend on one or two main elements, but in recent years, the development of high-entropy alloys has broken the status quo. High-entropy alloy is widely defined as an alloy system consisting of 5 to 13 major elements, with each element content between 5% and 35%, as proposed by Professor Yeh^{26–30} in 2004. Miracle³¹ et al. counted the top five alloy elements most studied at present, which are Fe, Ni, Co, Cr and Al. AlCoCrFeNi high-entropy alloy system is not only the most studied but also one of the earliest studied high-entropy alloy systems.³² The alloy has good mechanical properties.^{33–35} The microstructure and mechanical properties of AlCoCrFeNi alloy depend not only on the preparation process but also on the percentage of each element.^{36,37} Yeh³⁸ et al. prepared Al_xCoCrFeNi (x = 0 ~ 1.8) alloys with different aluminum contents by vacuum arc melting and studied the changing tendency of their phase compositions. The results show that the structure evolution with temperature can be divided into four types, and different types correspond to different structures. AlCoCrFeNi alloy has high heat resistance and can be used in aerospace applications.³⁹ AlCoCrFeNi alloy can be used in the coating field because of its high hardness, wear resistance, corrosion resistance and other excellent properties. Liu⁴⁰ et al. used laser remelting to improve the microstructure and wear resistance of AlCoCrFeNi high-entropy alloy coatings.

Based on the above research and considering the characteristics of high-entropy alloy, the single-phase AlCoCrFeNi high-entropy alloy foil with equal atomic ratio was introduced into the laminated composite system. The purpose of this research is to investigate the microstructure and mechanical properties of HEA-MIL composites. Initially, HEA-MIL composite was manufactured using hot pressing sintering technology. Then, the microstructure and phase composition of the material were analyzed and determined by scanning electron microscopy (SEM), electron backscattered diffraction (EBSD), energy-dispersive spectroscopy (EDS) and X-ray diffractometry (XRD). Finally, the compressive properties of the composite at room temperature were investigated.

EXPERIMENTAL PROCEDURES

Materials Fabrication

The novel HEA-MIL laminated composites were fabricated in this study through hot pressing sintering in a vacuum. The fabrication process involved using AlCoCrFeNi high-entropy alloy foil (50 × 50 × 1 mm), 1060 Al foil (50 × 50 × 0.5 mm) and TA1 foil (50 × 50 × 0.8 mm). The chemical composition of the starting materials used in this study is presented in Table I.

Prior to the experiment, titanium foil, aluminum foil and high-entropy alloy foil measuring 50 mm × 50 mm were polished using sandpaper to eliminate surface pollutants and oxides. Subsequently, all foils were cleaned in alcohol using an ultrasonic cleaning machine and then dried. The pretreated materials were arranged in the sequence of 'Ti-Al-AlCoCrFeNi-Al-Ti' before sintering. The schematic diagram of the stacked materials is depicted in Fig. 1. Finally, the stacked foils were placed in a vacuum hot pressing sintering furnace for the fabrication process.

In the process of hot-pressing sintering, the temperature is first raised to 630°C in 1 h, and the pressure of 3 MPa is maintained during the heating process to ensure good contact between layers. The temperature was then raised to 660°C at a rate of 1°C/min and kept at this temperature for 6 h to ensure complete reaction of aluminum with titanium or high-entropy alloy. During this process, the pressure is reduced to 0 MPa to prevent the liquid aluminum from being extruded. Finally, it is cooled to room temperature with the furnace, and the pressure of 3 MPa is restored.

Microstructure Characterization

The reaction products of HEA-MIL composite were analyzed using X'Pert PRO X-ray diffraction (XRD) for phase composition at a scanning speed of 4°min⁻¹ from 10° to 90°. Scanning electron

Table I. Chemical composition of raw materials

Materials	Composition (wt.%)
TA1	Ti: balance, Fe: 0.12, C: 0.047, N: 0.018, O: 0.153, H: 0.004
1060Al	Al: balance, Si:0.25, Cu:0.05, Zn:0.05, Mn:0.03, Mg:0.03, Fe:0.35, Ti:0.03, V:0.05
AlCoCrFeNi	Al: balance, Co:23.3, Cr:20.6, Fe:22.1, Ni:23.3

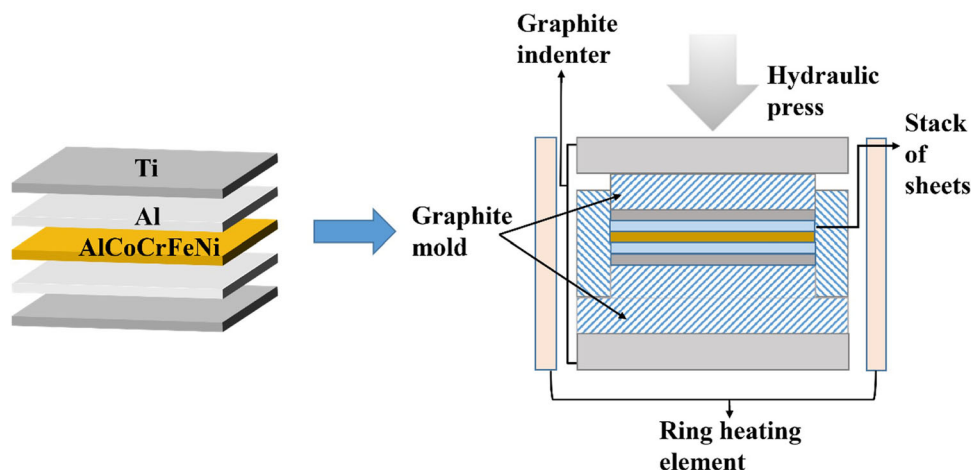


Fig. 1. Schematic diagram of stacked materials, including Ti foil, Al foil and AlCoCrFeNi foil.

microscopy Apreo C was used to characterize the microstructure of the composites. At the same time, the energy-dispersive spectrometer (EDS) attached to the scanning instrument was used to analyze the micro-domain composition of the alloy to characterize the distribution of each element in the composite material.

Mechanical Tests

The mechanical properties of HEA-MIL composites were tested by quasi-static compression test method. Mechanical tests were carried out on a universal testing machine (Instron 5500 R). The HEA-MIL composites were subjected to compression tests at room temperature at a strain rate of 0.01/s. The test directions are perpendicular to the laminate direction and parallel to the laminate direction. The information about the sample is plotted in Fig. 2.

RESULTS AND DISCUSSION

Microstructure Characterization

The detailed phase composition of the HEA-MIL composites was determined by XRD, as shown in Fig. 3a. The XRD patterns of HEA-MIL composites show that Al_3Ti is a newly formed intermetallic compound in addition to the original Ti phase, AlCoCrFeNi phase and residual Al phase during the preparation process. The high-entropy alloy still maintains BCC phase after hot pressing sintering. The main

reason for this phenomenon is that the AlCoCrFeNi high-entropy alloy has good structural stability and does not undergo phase transformation under the influence of temperature field and pressure field.

Figure 3b and c shows the overall microstructure of HEA-MIL laminate synthesized by hot-pressing sintering process and SEM images at the interface with high magnification. Figure 3b shows that the HEA-MIL composite is composed of alternating metal layers, including Ti layer, intermetallic compound layer, HEA-Al reaction layer and HEA layer. Compared with Ti/ Al_3Ti layered composites, HEA-MIL layered composites have two more layers and two more interfaces, and the reaction layer is the result of Al and high-entropy alloy diffusion. As Fig. 3c shows, at high magnification, the centerline defect is formed in the region between the intermetallic compound layer and reaction layer. The material's surface contains oxide, and as Al_3Ti grows, it breaks down when subjected to pressure. As the Al_3Ti layer thickens, the broken oxide is pushed towards the center of the original Al layer, resulting in the formation of a centerline.^{1,23} In addition, no obvious cracks were observed in the HEA-MIL composite, indicating that the process parameters for the preparation of HEA-MIL composite were reasonable, and the interface bonding formed was metallurgical bonding.

Figure 4 shows the distribution of chemical elements in the HEA-MIL composite as determined by EDS analysis. The analysis reveals that the

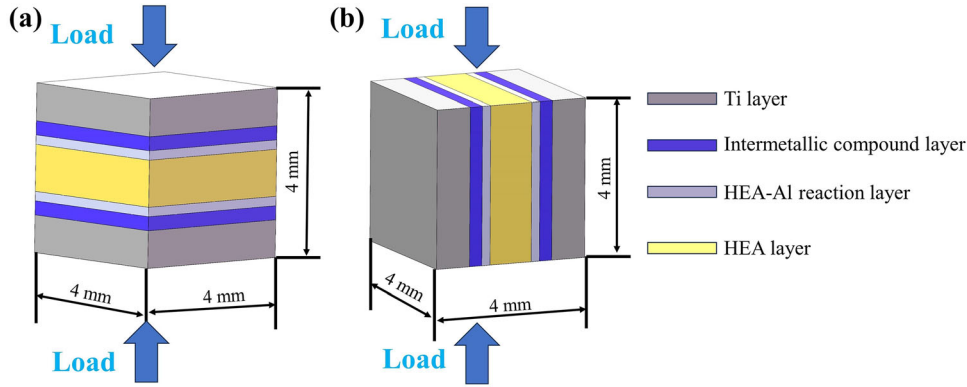


Fig. 2. Schematic diagram of HEA-MIL composite compressed sample, (a) load perpendicular to layer, (b) load parallel to layer.

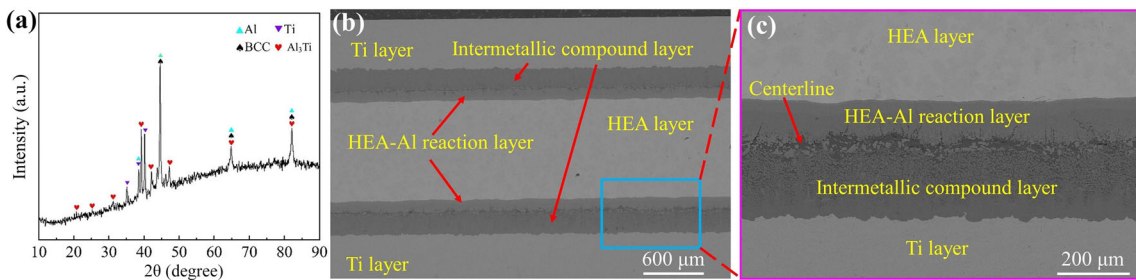


Fig. 3. XRD patterns and the typical structure of HEA-MIL composites: (a) XRD patterns, (b) low magnification SEM image, (c) high magnification SEM image.

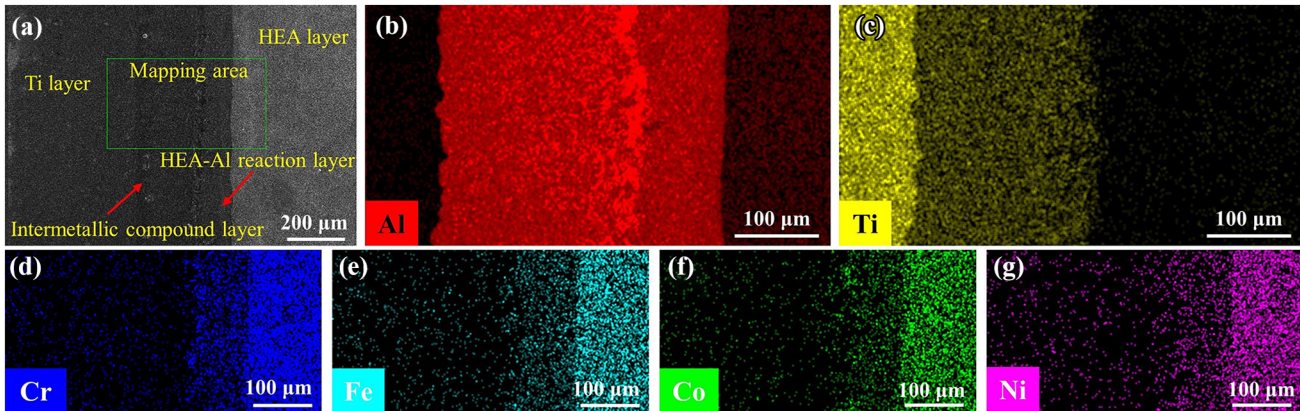


Fig. 4. SEM image and EDS element mapping of HEA-MIL composites, showing (a) microstructure, (b) Al, (c) Ti, (d) Cr, (e) Fe, (f) Co and (g) Ni element distributions.

reaction layer is predominantly composed of Al, along with Co, Cr, Fe and Ni elements. However, no new phase is observed in the XRD results. As the diffusion distance increases, the element content decreases, with only a small amount spreading to the other side of the centerline. In summary, compared to traditional Ti/Al₃Ti composites, the structure of the HEA-MIL composite is characterized by a more intricate arrangement of reaction layers and HEA layers within the Ti layer and intermetallic compound layer, resulting in a more complex layered structure.

EDS line scanning was used to study the distribution of elements near the interface of HEA-MIL composites, as shown in Fig. 5. Figure 5a shows the location of the EDS line scan, and Fig. 5b shows the distribution of each element. EDS analysis shows that the intermetallic compound layer is rich in Al and Ti elements, and the atomic ratio is about 3/1. Combined with XRD results, the intermetallic compound generated is Al₃Ti. In the reaction layer, Al element is the main element, with a small amount of high-entropy alloy elements, but the existence of the second phase cannot be determined only by the

distribution of elements. The elements in HEA layer are evenly distributed and basically maintain the original composition. To explore the diffusion of elements and determine the chemical composition in each layer, EDS point scanning was performed, and the results are shown in Table II.

To further investigate the new products introduced into Ti/Al₃Ti layered composites by high-entropy alloys, EBSD analysis was conducted. The EBSD test area was selected to include the high-entropy alloy layer and the adjacent HEA-Al reaction layer. The EBSD analysis results are shown in Fig. 6. It is important to note that only the HEA layer has EBSD analysis results, as the reaction layer experiences lattice distortion due to stress concentration.

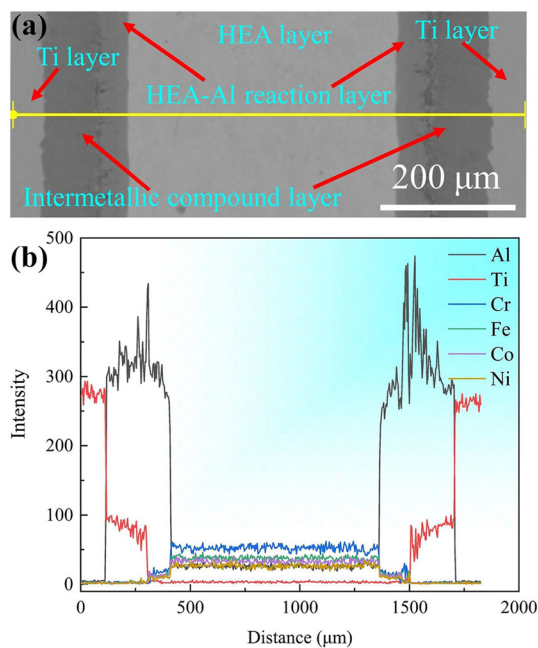


Fig. 5. EDS line scanning of HEA-MIL composites, (a) microscopic morphology, (b) distribution of each element.

Figure 6a displays the phase map of the AlCoCrFeNi alloy. The red area indicates the presence of the BCC phase structure, while the blue area represents the FCC phase. The figure reveals that the AlCoCrFeNi alloy primarily consists of the BCC phase, with some smaller grains forming a minor FCC phase at the edge, without a distinct boundary. This occurrence is attributed to the sintering process, during which a portion of the BCC phase of the AlCoCrFeNi alloy undergoes a transition to the FCC phase under the influence of the temperature field. However, due to the limited reaction time, this transition is not significantly pronounced. Fig. 6b is the grain boundary map, in which high-angle grain boundary is represented by black lines and low-angle grain boundary by green lines. The figure shows a higher percentage of high-angle grain boundaries. When cracks extend to the location of high-angle grain boundaries, higher energy is required to overcome the grain boundaries, which gives the material a higher strength. Figure 6c is the statistical chart of grain size and shows that there are large grains on the whole, with large size differences and concentrated distribution in the range of 30–75 μm. Figure 6d and e shows the local average misorientation (LAM) map and its corresponding statistical figure, respectively. The different colors in the map represent various distributions of orientation difference, with the color red indicating a greater orientation difference. The figure reveals that the blue color predominates throughout the area, indicating that the orientation difference within the HEA layer is minimal. This suggests that the degree of plastic deformation, defect density and internal stress distribution are all low, and there is no noticeable stress concentration. Figure 6f and g shows the grain orientation spread (GOS) map and its statistical diagram, respectively. Different colors depend on the lattice distortion intensity. The closer the color is to blue, the lower the dislocation density will be. The figure shows that blue occupies most of the region, which means that the grain strain in this region is small overall, and only a few have large

Table II. Typical chemical compositions of each layer and phase detected by EDS

	Element	HEA layer	Reaction layer	Intermetallic layer	Ti layer
wt. %	Ti	0.02	0.08	27.62	99.20
	Al	8.58	63.60	71.10	0.14
	Co	24.40	10.51	0.39	0.34
	Cr	21.26	8.37	0.56	0.07
	Fe	22.48	9.17	0.20	0.25
	Ni	23.27	8.27	0.13	0.00
Summation at. %	–	100	100	100	100
	Ti	0.02	0.05	17.83	99.19
	Al	16.39	78.49	81.45	0.25
	Co	21.34	5.94	0.21	0.29
	Cr	21.07	5.36	0.33	0.06
	Fe	20.75	5.47	0.11	0.21
Summation	Ni	20.43	4.69	0.07	0.00
	–	100	100	100	100

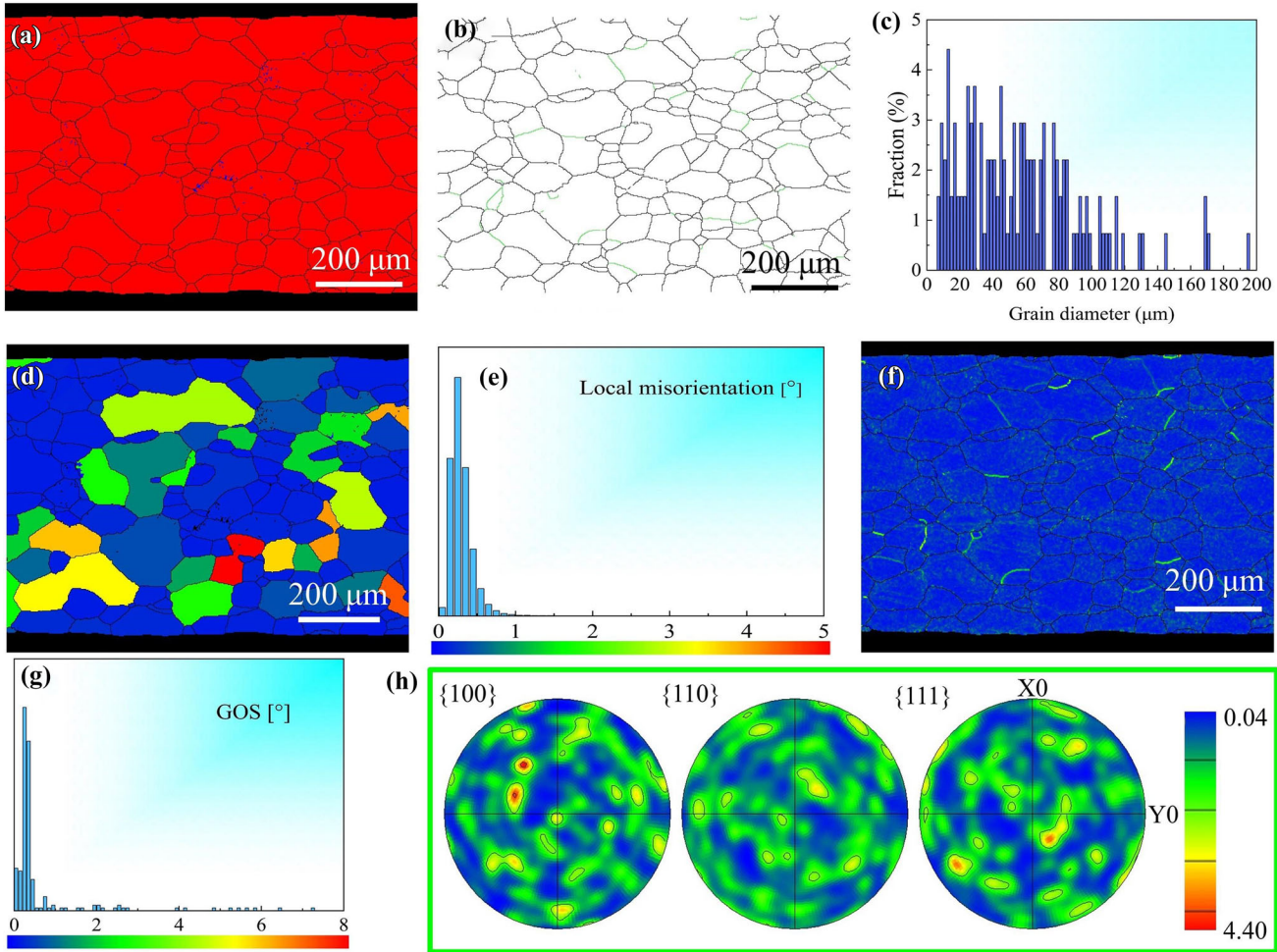


Fig. 6. EBSD analysis results: (a) the phase map, (b) grain boundary map, (c) statistical chart of grain size, (d) the local average misorientation map, (e) statistical chart of local misorientation, (f) the grain orientation spread (GOS), (g) statistical chart of GOS, (h) the pole figure (Color figure online).

strain. Figure 6h shows the pole figure (PF), which reveals that the regions with low polar density are primarily found on the three surfaces $(1\ 0\ 0)$, $(1\ 1\ 0)$ and $(1\ 1\ 1)$. The distribution of these regions is relatively uniform, and the overall texture strength is low. This suggests that the grains' texture strength is weak and dispersed during sintering, indicating that they do not have a significant impact on the diffusion process. This observation aligns with the description of the hysteretic diffusion effect of high-entropy alloys.

Compression Properties

To investigate the mechanical properties of HEA-MIL composites, compression tests were conducted. Figure 7 illustrates the stress-strain curves of HEA-MIL composites under different loading directions. When the load is applied perpendicular to the layers, the compressive strength of the HEA-MIL composite is measured at 1359.61 MPa with a failure strain of 41.53%. When the load is parallel

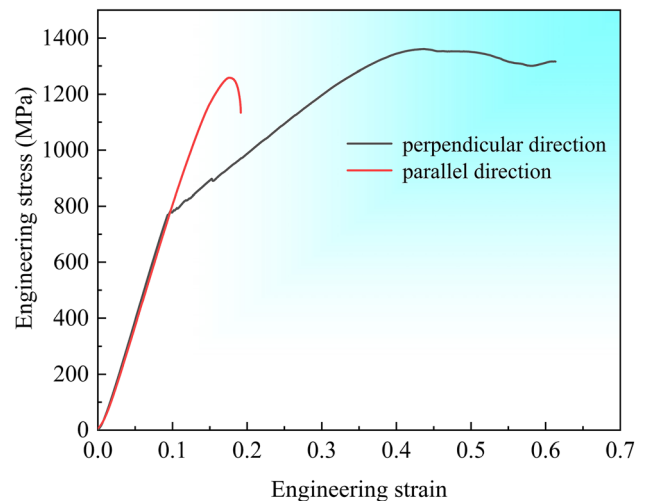


Fig. 7. Typical compressive engineering stress-strain curves of composites, including load perpendicular to layers and parallel to layers.

Table III. Results of HEA-MIL composites after quasi-static compression tests

Load direction	Number	Compressive strength (MPa)	Failure strain (%)
Perpendicular	1	1360.24	41.41
	2	1354.95	41.62
	3	1363.64	41.55
Average	—	1359.61	41.53
Parallel	1	1258.21	17.91
	2	1263.56	17.85
	3	1253.63	17.76
Average	—	1258.47	17.84

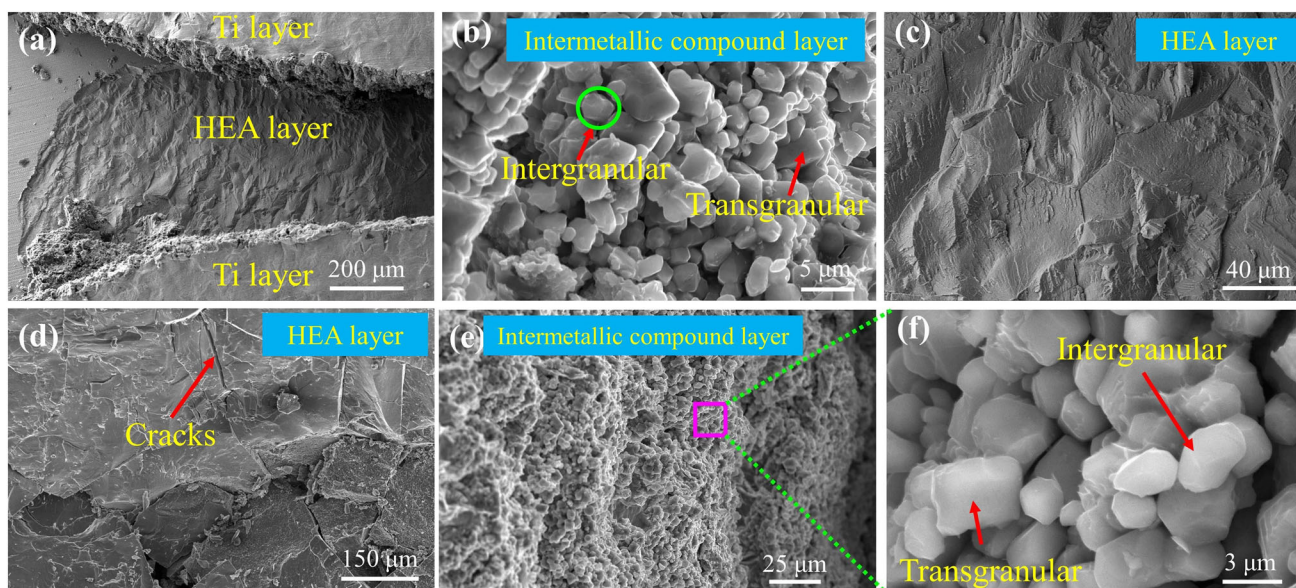


Fig. 8. Typical microscopic morphology of composites under perpendicular (a-c) and parallel (d-f) loads to the layers: (a) overall morphology, (b) fracture morphology of the intermetallic compound layer, (c) fracture morphology of the HEA layer, (d) cracks on the HEA layer, (e) intermetallic compound layer debonding surface morphology, (f) intergranular and transgranular fracture of Al_3Ti .

to the layers, the compressive strength is 1258.47 MPa, and the failure strain is 17.84%. Detailed data can be found in Table III. As depicted in Fig. 8, the compression curves for loads perpendicular to and parallel to the layers exhibit notable differences. The findings indicate that when the load is applied perpendicular to the layers, the composite material initially undergoes elastic deformation. Subsequently, the brittle layer experiences brittle fracture, while the Ti layer continues to undergo plastic deformation and expands. In the final stage, the sample extrudes the brittle layer under the load until it becomes thin, leading to the termination of the test. The Ti layer of the HEA-MIL composite is surrounded by a brittle layer on both sides, giving the specimen a plastic appearance as a whole. However, when the load is applied parallel to the lamination direction, each layer of the composite material simultaneously bears the load and fails immediately after the elastic deformation stage. Under the action of the load, the

HEA-MIL composites experience stratified fracture, causing the brittle layer to break into small irregular fragments that are challenging to observe using scanning electron microscopy.

To investigate the form of failure of HEA-MIL composites under compressive loading, we observed the microscopic morphology of compressed specimens after compression tests. Figure 8a, b, and c displays the fracture morphology in the perpendicular direction. Figure 8a provides an overview of the sample's side, revealing the stratification phenomenon and characteristics of plastic deformation on the Ti layer's surface. Figure 8b shows the fracture morphology of the intermetallic compound layer, specifically Al_3Ti , demonstrating both inter- and transgranular forms of fracture for Al_3Ti . The fracture morphology of the HEA layer is shown in Fig. 8c, with a flat fracture surface indicating typical brittle fracture. Figure 8d, e, and f displays the fracture morphologies in parallel directions. Figure 8d reveals numerous cracks in the HEA

Table IV. Compressive properties compared with other works

Material	Compressive strength (MPa)	Failure strain (%)
AlCoCrFeNi (mechanical alloying + SPS) ⁴¹	1900	11.6
AlCoCrFeNi (vacuum arc melting) ⁴²	2004	32.7
Ti/Al ₃ Ti (perpendicular) ⁴³	1300	3.6
Ti/Al ₃ Ti (parallel) ⁴³	1030	3.4

layer. Figure 8e and f illustrates the fracture morphology and a magnified view of the intermetallic compound layer, respectively. Figure 8f demonstrates that the fracture form of Al₃Ti exhibits both inter- and transgranular characteristics.

Combining Tables III with IV shows that the compressive strength of HEA-MIL composites decreases, while the plastic deformation capacity improves compared to AlCoCrFeNi high-entropy alloys. However, compared to Ti/Al₃Ti laminated composites, the compressive strengths in both the parallel and perpendicular directions to the layers have increased. This is particularly noticeable for the load parallel to the layers, indicating that the high-entropy alloy AlCoCrFeNi has the ability to strengthen the Ti/Al laminated composites.

In conclusion, the compression tests show that the new HEA-MIL composites have good mechanical properties and great potential in engineering applications. Based on our previous research, using TC4 instead of TA1 can effectively improve the mechanical properties of the material. In addition, the thickness of the metal layer can be changed to improve its performance, which will be the focus of our subsequent work.

CONCLUSION

Novel high-entropy alloy-reinforced Ti/Al metallic-intermetallic laminated composite was prepared by vacuum hot pressing sintering. The microstructure, compression behavior and fracture mechanism of HEA-MIL composites were studied. The main conclusions reached so far are summarized as follows:

- (1) Following the vacuum hot pressing sintering process, the HEA-MIL composite exhibits a distinctive multi-level symmetric structure, characterized by alternating combinations of dissimilar metal layers. Analyzing the composite through XRD and EDS techniques revealed that the intermetallic compound layer primarily consists of the Al₃Ti phase. Additionally, EBSD analysis indicated that the inner HEA layer remains unaffected by the sintering process, retaining its BCC structure with a large grain size and no stress concentration.
- (2) The compression test of HEA-MIL composites demonstrates that this type of laminated

composite exhibits a balance between strength and plasticity. In the case where the load is applied perpendicular to the lamination direction, the compression peak value of HEA-MIL composites is measured to be 1359.61 MPa, with a failure strain of 41.53%. When the load is parallel to the lamination direction, the compression peak value of HEA-MIL composites increases to 1258.47 MPa, accompanied by a failure strain of 17.84%.

- (3) Regardless of whether the load is parallel or perpendicular to the layer, the HEA layer and intermetallic layer predominantly undergo brittle fractures, whereas the Ti layer demonstrates typical plastic deformation.

ACKNOWLEDGEMENTS

This work was supported by the Natural Science Foundation of China (Grant No. 51901058), the “Ten Million” Major Project of Heilongjiang Province, China (Grant No. 2020ZX03A03) and the Natural Science Foundation of Heilongjiang Province, China (Grant No. LH2020E084).

CONFLICT OF INTERESTS

The authors declare that they have no conflict of interest.

REFERENCES

1. D.J. Harach and K.S. Vecchio, *Metall. Mater. Trans. A* 32, 1493 <https://doi.org/10.1007/s11661-001-0237-0> (2001).
2. Y. Cao, C.H. Guo, S.F. Zhu, N.J. Wei, R.A. Javed, and F.C. Jiang, *Mater. Sci. Eng. A* 637, 235 <https://doi.org/10.1016/j.msea.2015.04.025> (2015).
3. P.J. Zhou, C.H. Guo, E.H. Wang, Z.M. Wang, Y. Chen, and F.C. Jiang, *Mater. Sci. Eng. A* 665, 66 <https://doi.org/10.1016/j.msea.2016.04.020> (2016).
4. R.D. Price, F.C. Jiang, R.M. Kulin, and K.S. Vecchio, *Mater. Sci. Eng. A* 528, 3134 <https://doi.org/10.1016/j.msea.2010.12.087> (2011).
5. I.A. Bataev, A.A. Bataev, V.I. Mali, and D.V. Pavliukova, *Mater. Des.* 35, 225 <https://doi.org/10.1016/j.matdes.2011.09.030> (2012).
6. F.W. Kang, X.M. Zhang, F.H. Zhang, E.H. Wang, Y. Cao, W. Jiang, L.P. Wang, Y.Q. Han, and C.F. Lin, *Mater. Res. Express* 8, 1 <https://doi.org/10.1088/2053-1591/ac0558> (2021).
7. J.C. Rawers and D.E. Alman, *Compos. Sci. Technol.* 54, 379 [https://doi.org/10.1016/0266-3538\(95\)00072-0](https://doi.org/10.1016/0266-3538(95)00072-0) (1995).
8. J.C. Rawers and K. Perry, *J. Mater. Sci.* 31, 3501 <https://doi.org/10.1007/BF00360755> (1996).
9. K.S. Vecchio, *JOM* 57, 25 <https://doi.org/10.1007/s11837-005-0229-4> (2005).

10. R.A. Raghavendra, K.S. Vecchio, F.C. Jiang, and A. Rohatgi, *Metall. Mater. Trans. A* 36, 1595 <https://doi.org/10.1007/s11661-005-0251-8> (2005).
11. R.A. Raghavendra, K.S. Vecchio, F.C. Jiang, and A. Rohatgi, *Metall. Mater. Trans. A* 36, 3217 <https://doi.org/10.1007/s11661-005-0092-5> (2005).
12. G. Yu, H.M. Wang, S.H. Chen, L. Wei, J.H. Huang, J. Yang, and Z.Y. Zhao, *Mater. Charact.* 159, 110043 <https://doi.org/10.1016/j.matchar.2019.110043> (2020).
13. B. Wang, D.J. Wang, J. Zhao, H.W. Ning, and G. Liu, *Mater. Sci. Eng. A* 827, 142050 <https://doi.org/10.1016/j.msea.2021.142050> (2021).
14. X. Li, Y.H. Sun, Z.Q. Wang, and F.C. Jiang, *J. Alloys Compd.* 774, 656 <https://doi.org/10.1016/j.jallcom.2018.10.074> (2018).
15. F.C. Jiang, X. Li, Z.Q. Wang, C.H. Guo, and J.D. Wang, *J. Alloys Compd.* 843, 156065 <https://doi.org/10.1016/j.jallcom.2020.156065> (2020).
16. Y. Tian, E.H. Wang, W. Li, Z.Y. Niu, Y.P. Chang, C.H. Guo, Z.Q. Wang, Z. Leng, and F.C. Jiang, *J. Alloys Compd.* 739, 669 <https://doi.org/10.1016/j.jallcom.2017.12.258> (2018).
17. F.F. Jiao, M.Y. Liu, F.C. Jiang, J.Y. Zhao, P. Li, and Z.Q. Wang, *Mater. Sci. Eng. A* 765, 138225 <https://doi.org/10.1016/j.msea.2019.138225> (2019).
18. Y.P. Chang, Z.Q. Wang, X.C. Li, Z. Leng, C.H. Guo, Z.Y. Niu, and F.C. Jiang, *Intermetallics* 112, 106544 <https://doi.org/10.1016/j.intermet.2019.106544> (2016).
19. C.F. Lin, S.Y. Wang, H.R. Yan, Y.Q. Han, J.Y. Zhu, and H. Shi, *Met. Mater. Int.* 27, 306 <https://doi.org/10.1007/s12540-020-00724-7> (2021).
20. E.H. Wang, C.H. Guo, P.J. Zhou, C.F. Lin, X.X. Han, and F.C. Jiang, *Mater. Des.* 95, 446 <https://doi.org/10.1016/j.matdes.2016.01.130> (2016).
21. E.H. Wang, Y. Tian, Z.Q. Wang, F.F. Jiao, C.H. Guo, and F.C. Jiang, *J. Alloys Compd.* 696, 1059 <https://doi.org/10.1016/j.jallcom.2016.12.062> (2017).
22. E.H. Wang, F.W. Kang, H.B. Wang, Y. Cao, and F.C. Jiang, *J. Alloys Compd.* 775, 1307 <https://doi.org/10.1016/j.jallcom.2018.10.277> (2019).
23. Y.Q. Han, F.C. Jiang, C.F. Lin, D. Yuan, H. Huang, E.H. Wang, Z.Q. Wang, and C.H. Guo, *J. Alloys Compd.* 729, 1145 <https://doi.org/10.1016/j.jallcom.2017.09.267> (2017).
24. Y.Q. Han, Q.H. Que, R. Cheng, C.F. Lin, W.Q. Han, E.H. Wang, J. Zhu, and H.R. Yan, *Met. Mater. Int.* 27, 4035 <https://doi.org/10.1007/s12540-020-00942-z> (2021).
25. Y.Q. Han, R. Cheng, C.F. Lin, E.H. Wang, Y. Wang, L.J. Song, and W.Q. Han, *J. Alloys Compd.* 881, 160520 <https://doi.org/10.1016/j.jallcom.2021.160520> (2021).
26. T.K. Chen, M.S. Wong, T.T. Shun, and J.W. Yeh, *Surf. Coat. Technol.* 200, 1219 <https://doi.org/10.1016/j.surfcoat.2005.08.081> (2004).
27. C.Y. Hsu, J.W. Yeh, S.K. Chen, and T.T. Shun, *Metall Mater Trans A* 35, 1465 <https://doi.org/10.1007/s11661-004-0254-x> (2004).
28. P.K. Huang, J.W. Yeh, T.T. Shun, and S.K. Chen, *Adv Eng Mater.* 2004(6), 74 <https://doi.org/10.1002/adem.200300507> (2004).
29. J.W. Yeh, S.J. Lin, T.S. Chin, J.Y. Gan, S.K. Chen, T.T. Shun, C.H. Tsau, and S.Y. Chou, *Metall Mater Trans A* 35, 2533 <https://doi.org/10.1007/s11661-006-0234-4> (2004).
30. J.W. Yeh, S.K. Chen, S.J. Lin, J.Y. Gan, T.S. Chin, T.T. Shun, C.H. Tsau, and S.Y. Chang, *Adv Eng Mater.* 6, 299 <https://doi.org/10.1002/adem.200300567> (2004).
31. D.B. Miracle and O.N. Senkov, *Acta Mater.* 122, 1 <https://doi.org/10.1016/j.actamat.2016.08.081> (2017).
32. M. Tokarewicz and M. Grdzka-Dahlke, *Metals* 11, 1302 <https://doi.org/10.3390/met11081302> (2021).
33. F.J. Wang, Y. Zhang, G.L. Chen, and H.A. Davies, *J. Eng. Mater. Technol.* 131, 034501 <https://doi.org/10.1115/1.3120387> (2009).
34. H.P. Chou, Y.S. Chang, S.K. Chen, and J.W. Yeh, *Mater. Sci. Eng. B* 163, 184 <https://doi.org/10.1016/j.mseb.2009.05.024> (2009).
35. P.Y. Shi, Y. Yu, N.N. Xiong, M.Z. Liu, Z.H. Qiao, G.W. Yi, Q.Q. Yao, G.P. Zhao, E.Q. Xie, and Q.H. Wang, *Tribol. Int.* 151, 106470 <https://doi.org/10.1016/j.triboint.2020.106470> (2020).
36. T.T. Shun and W.J. Hung, *Adv. Mater. Sci. Eng.* 1, 1 <https://doi.org/10.1155/2018/5826467> (2018).
37. L. Guo, D.H. Xiao, W.Q. Wu, S. Ni, and M. Song, *Intermetallics* 103, 1 <https://doi.org/10.1016/j.intermet.2018.09.011> (2018).
38. W.R. Wang, W.L. Wang, and J.W. Yeh, *J. Alloys Compd.* 589, 143 <https://doi.org/10.1016/j.jallcom.2013.11.084> (2014).
39. K.R. Lim, K.S. Lee, J.S. Lee, J.Y. Kim, H.J. Chang, and Y.S. Na, *J. Alloys Compd.* 728, 1235 <https://doi.org/10.1016/j.jallcom.2017.09.089> (2017).
40. Q. Liu, T.S. Dong, B.G. Fu, G.L. Li, and L.J. Yang, *J. Mater. Eng. Perform.* 30, 5728 <https://doi.org/10.1007/s11665-021-05806-0> (2021).
41. W. Ji, Z.Y. Fu, W.M. Wang, H. Wang, J.Y. Zhang, Y.C. Wang, and F. Zhang, *J. Alloys Compd.* 589, 61–66 <https://doi.org/10.1016/j.jallcom.2013.11.146> (2014).
42. Y.P. Wang, B.S. Li, M.X. Ren, C. Yang, and H.Z. Fu, *Mater. Sci. Eng. A* 491, 154 <https://doi.org/10.1016/j.msea.2008.01.064> (2008).
43. C.F. Lin, F.C. Jiang, Y.Q. Han, E.H. Wang, D. Yuan, and C.H. Guo, *J. Alloys Compd.* 743, 52–62 <https://doi.org/10.1016/j.jallcom.2018.01.392> (2018).

Publisher's Note Springer Nature remains neutral with regard to jurisdictional claims in published maps and institutional affiliations.

Springer Nature or its licensor (e.g. a society or other partner) holds exclusive rights to this article under a publishing agreement with the author(s) or other rightsholder(s); author self-archiving of the accepted manuscript version of this article is solely governed by the terms of such publishing agreement and applicable law.